

# Atomic Raman scattering: Third-order diffraction in a double geometry

Sabrina Hartmann,<sup>1</sup> Jens Jenewein,<sup>1</sup> Sven Abend,<sup>2</sup> Albert Roura,<sup>3</sup> and Enno Giese<sup>1</sup>

<sup>1</sup>*Institut für Quantenphysik and Center for Integrated Quantum Science and Technology (IQ<sup>ST</sup>), Universität Ulm, Albert-Einstein-Allee 11, D-89069 Ulm, Germany*

<sup>2</sup>*Institut für Quantenoptik, Leibniz Universität Hannover, Welfengarten 1, D-30167 Hannover, Germany*

<sup>3</sup>*Institute of Quantum Technologies, German Aerospace Center (DLR), Söflinger Straße 100, D-89077 Ulm, Germany*

In a retroreflective scheme atomic Raman diffraction adopts some of the properties of Bragg diffraction due to additional couplings to off-resonant momenta. As a consequence, double Raman diffraction has to be performed in a Bragg-type regime. Taking advantage of this regime, double Raman allows for resonant higher-order diffraction. We study theoretically the case of third-order diffraction and compare it to first order as well as a sequence of first-order pulses giving rise to the same momentum transfer as the third-order pulse. In fact, third-order diffraction constitutes a competitive tool for the diffraction of ultracold atoms and interferometry based on large momentum transfer since it allows to reduce the complexity of the experiment as well as the total duration of the diffraction process compared to a sequence.

## I. INTRODUCTION

Higher-order Bragg diffraction [1–5] in combination with sequential pulses [6, 7] has become a standard tool for large-momentum-transfer (LMT) techniques to enhance the sensitivity of light-pulse atom interferometers [8, 9]. However, with Raman diffraction [8, 10, 11], the other main mechanism, only sequential pulses [12–14] have routinely been employed so far. In this article, we extend Raman in a double-diffraction geometry [15–17] to also allow for higher-order diffraction and study the efficiency compared to a standard first-order sequence. Such a setup retains the possibility of state-selective detection, while being more efficient and less complex than a sequence of first-order pulses for narrow momentum distributions.

Bloch oscillations [18–22], higher-order diffraction [1–5], and sequential pulses [6, 7, 12–14, 23] are some of the most commonly used techniques used for LMT applications based on Bragg diffraction. They are complemented by double diffraction [2, 6, 15–17], where an atom at rest diffracts from two counterpropagating light gratings in two opposite directions. The latter is particularly well suited for experiments under microgravity conditions [24–30] or for horizontal geometries [31, 32]. Due to its symmetry, laser phases are not imprinted on the two branches of the interferometer, and similar noise sources are intrinsically suppressed [2, 6, 12]. Even though many applications of double diffraction focus on Bragg, the geometry was first pioneered for Raman and is still used to date as one of the few LMT techniques for Raman diffraction, together with sequential pulses. However, one of the benefits of double Raman diffraction has not been explored so far, namely the possibility to scatter into higher diffraction orders.

In contrast to single Raman, which can be described as a closed two-level system, off-resonant couplings appear in single Bragg diffraction [33, 34], limiting the operation to the Bragg regime but at the same time allowing for higher-order diffraction [35]. The additional grating

in double diffraction induces further off-resonant transitions for both Raman and Bragg diffraction. As a consequence, the application of Raman diffraction is restricted to a Bragg-type regime as well. In double Bragg diffraction resonant and off-resonant couplings at the same momentum state appear causing a more complex diffraction behavior [35, 36]. However, these features do not appear in double Raman diffraction, which therefore constitutes a simpler diffraction mechanism.

In this article we demonstrate that third-order double Raman diffraction with high efficiency is possible, although it is more velocity selective than its first-order counterpart. However, for narrow momentum distributions like the ones associated with Bose-Einstein condensates (BECs) it can be a competitive alternative to a pulse sequence when the duration of the beam splitting process is limited.

In Sec. II we recall first-order double Raman diffraction with a Gaussian pulse shape as well as sequential Doppler-detuned single-diffraction with typical box-shaped pulses to calculate the efficiency of an LMT beam splitter. Such a combination of Gaussian and box-shaped pulses constitutes a good compromise between diffraction efficiency and overall duration of the sequence. We then perform in Sec. III an analysis of third-order Raman diffraction and show that even though its efficiency is inherently worse than a comparable first-order pulse, it can be better than that of the sequence. We conclude with a brief discussion in Sec. IV. For completeness, the general set of differential equations for double Raman diffraction is given in the Appendix.

## II. FIRST-ORDER DIFFRACTION

### A. Double Raman diffraction

An atom at rest interacts with two strongly detuned optical gratings (with a detuning much larger than the linewidth) that move in opposite directions, each one

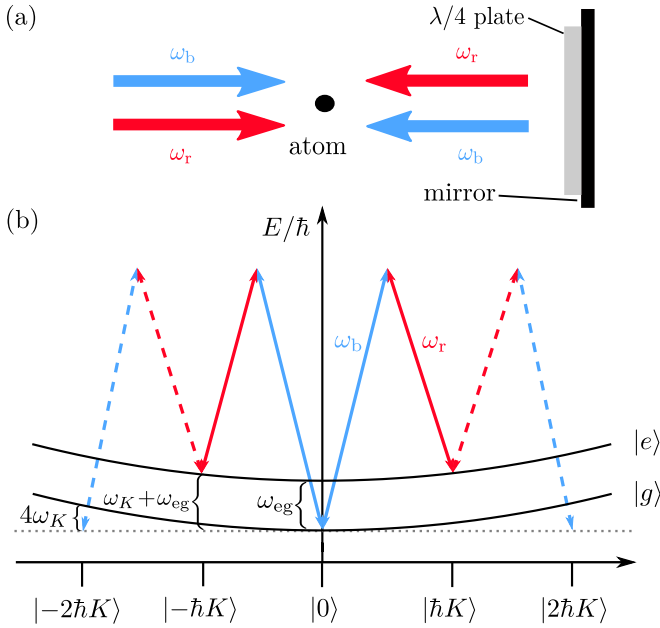


FIG. 1. Schematic setup with an atom at rest ( $p_0 = 0$ ) in a retroreflective geometry built by a  $\lambda/4$  plate and a mirror (a). The atom diffracts from two counterpropagating optical gratings (upper and lower pair of light fields, respectively), absorbs a photon with frequency  $\omega_b$  and emits a photon  $\omega_r$  in opposite direction from each grating. This process causes a total recoil of  $\pm\hbar K$  with  $K = (\omega_b + \omega_r)/c$  and by that leads to a gain of kinetic energy  $\hbar\omega_K$ . The energy-momentum diagram in (b) shows that such a process is resonant if the energy difference between the light fields  $\hbar\Delta\omega \equiv \hbar(\omega_b - \omega_r)$  equals the energy difference  $\hbar\omega_{eg}$  between the atomic ground  $|g\rangle$  and excited state  $|e\rangle$  in addition to the recoil energy  $\hbar\omega_K$ . Resonant processes start and end on the parabola (solid arrows), off-resonant processes are denoted by dashed arrows.

generated by counterpropagating light fields of frequencies  $\omega_b$  and  $\omega_r$ , see Fig. 1(a). The gratings can be distinguished by their polarization [12], so that within a retroreflective setup, where both light fields are guided from one side to the atom and retroreflected at the other side, the polarizations have to be rotated by a  $\lambda/4$  plate [6, 12] to suppress spurious standing waves. The diffraction process can be understood in terms of absorbing a photon with frequency  $\omega_b$  and subsequently emitting a photon with frequency  $\omega_r$  in the opposite direction from each grating. This process causes a total momentum recoil of  $\pm\hbar K$  for the two gratings, with  $K \equiv (\omega_b + \omega_r)/c$ , and the atom gains a kinetic energy  $\hbar\omega_K$ , in terms of the recoil frequency

$$\omega_K = \frac{\hbar K^2}{2M}, \quad (1)$$

where  $M$  is the atomic mass.

The diffraction process is determined by the transferred energy, i.e. by the difference of the laser frequencies  $\Delta\omega \equiv \omega_b - \omega_r$ . A transition that is resonant for first-order diffraction corresponds in Fig. 1(b) to the

case where the solid arrows start and end on a parabola, the kinetic energy of an internal state. This is possible if  $\hbar\Delta\omega$  equals the kinetic energy  $\hbar\omega_K$  gained through recoil plus the energy difference  $\hbar\omega_{eg}$  between internal ground  $|g\rangle$  and excited state  $|e\rangle$ , i.e.

$$\Delta\omega = \omega_{eg} + \omega_K. \quad (2)$$

Since the AC Stark shift can in principle be compensated, we refrain from including it in the subsequent discussion or the resonance condition.

The two gratings allow simultaneous diffraction in opposite directions but also enable spurious off-resonant transitions to higher diffraction orders denoted by dashed arrows. Additional couplings through polarization imperfections are neglected throughout this article. Moreover, we assume plane waves and neglect wave front distortions.

The diffraction process depicted in Fig. 1(b) is described by the truncated system of differential equations

$$\dot{g}_0 = i\Omega e^{-i\omega_D t} e_1 + i\Omega e^{i\omega_D t} e_{-1} \quad (3a)$$

$$\dot{e}_{\pm 1} = i\Omega e^{\mp i\omega_D t} e^{-i4\omega_K t} g_{\pm 2} + i\Omega e^{\pm i\omega_D t} g_0, \quad (3b)$$

coupling the ground state probability amplitudes  $g_n \equiv g(p + n\hbar K)$  for the momentum eigenstate  $|p + n\hbar K\rangle$  to the excited state amplitudes  $e_n \equiv e(p + n\hbar K)$ . The system of equations is derived from the generalized version of the differential equations describing double Raman diffraction presented in the Appendix. Rabi oscillations take place between the probability amplitude  $g_0$  of the ground state and those of the excited state with two different momenta,  $e_1$  and  $e_{-1}$ . At the same time, the probability amplitudes of the excited states  $e_{\pm 1}$  couple off-resonantly to  $g_{\pm 2}$  indicated with a detuning  $4\omega_K$ . These kind of transitions are prominent in the *Raman-Nath* (*Kapitza-Dirac*) regime [35, 37] where  $\Omega/\omega_K \gtrsim 1$ , but are suppressed in the *Bragg*-type regime with  $\Omega/\omega_K \ll 1$  in which double Raman is typically performed. Note that  $e_{\pm 2}$  couples further to higher diffraction orders, but these transitions are even more off-resonant and therefore suppressed in the Bragg-type regime. The Doppler frequency  $\omega_D = pK/M$  corresponds to the deviation from the resonant momentum  $p = 0$  within a wave packet and acts as a detuning to the resonant transition, leading to the effect of *velocity selectivity* [10, 11, 38–40]. As coupling strength  $\Omega(t) \propto \Omega_0 \exp[-t^2/(2\Delta\tau^2)]$  we consider a Gaussian function of width  $\Delta\tau$ .

The coupling strength is connected to the pulse area  $A$  via

$$A = \int dt \sqrt{2} \Omega(t). \quad (4)$$

An area of  $A = \pi/2$  leads to the transition  $|g, 0\rangle \rightarrow (|e, \hbar K\rangle + |e, -\hbar K\rangle)/\sqrt{2}$ , creating a superposition of left- and right-moving wave-packet components and therefore corresponds to a double-Raman beam splitter.

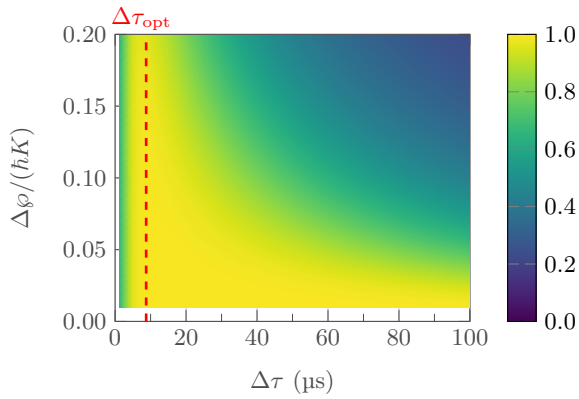


FIG. 2. Efficiency  $\mathcal{E}_{\pm 1}^0$  for a first-order double-diffraction beam splitter as a function of the width of the initial wave function  $\Delta\phi$  and the pulse duration  $\Delta\tau$  for a Gaussian pulse shape. Higher order diffraction appears in the Raman-Nath regime (drop in efficiency for small  $\Delta\tau$ ), for higher  $\Delta\tau$  losses are determined by velocity selectivity.

### 1. Numerical treatment

We numerically solve the system of differential equations Eq. (18) using the corresponding resonance condition Eq. (2) for Rb<sup>87</sup> with MATLAB's ODE45, a Runge-Kutta algorithm, with relative accuracy  $10^{-3}$  and absolute accuracy  $10^{-6}$ . We calculate a transition function  $G_{\Delta\tau}(p_f, p_i)$  which connects the initial and final momentum eigenstates [36]. The transition function can be applied to the initial Gaussian wave packet  $\psi_i(p_i) \propto \exp[-(p_i - p_0)^2 / (4\Delta\phi^2)]$  with  $p_0 = 0$  to obtain the final wave function

$$\psi_f(p_f) = \int dp_i G_{\Delta\tau}(p_f, p_i) \psi_i(p_i). \quad (5)$$

We truncate the range of momenta so that the solution for the diffraction efficiency (discussed in the following paragraph) obtained with  $n_{\max}$  and  $n_{\max+1}$  is at most of the same magnitude as the solver accuracy.

### 2. Diffraction Efficiency

We define the efficiency of an  $n$ th-order symmetric diffraction process between the momenta  $|\pm n_0 \hbar K\rangle$  and  $|\pm(n_0 + n) \hbar K\rangle$  as

$$\mathcal{E}_{\pm n}^{n_0} = \int_{p_-}^{p_+} dp_f |\psi_f(p_f)|^2 + \int_{-p_+}^{-p_-} dp_f |\psi_f(p_f)|^2 \quad (6)$$

with the integration range  $p_{\pm} = (n_0 + n \pm 1/2)\hbar K$  and  $n, n_0 \in \mathbb{N}$ . Even though the expression works for arbitrary initial momenta, we have restricted ourselves to integer momenta  $p_0 = n_0 \hbar K$  that are relevant for sequences of pulses.

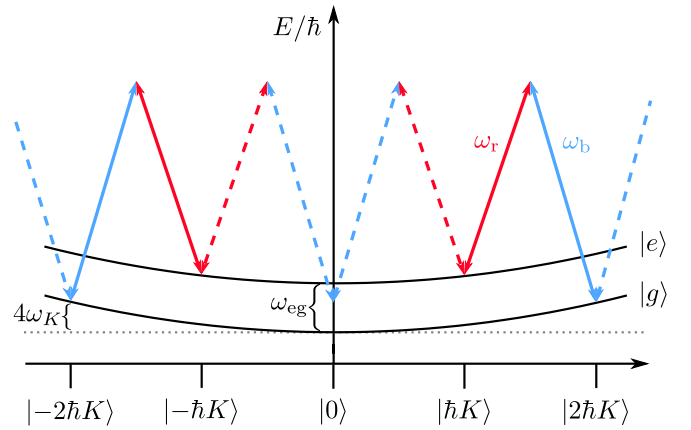


FIG. 3. Energy-momentum diagram and resonant transitions for an atom with initial momentum  $p_0 = \hbar K$  (solid arrows) and initially in the excited state. The Doppler detuning of the spurious grating suppresses off-resonant transitions (dashed arrows), turning double into single diffraction. The initial conditions are chosen so that they correspond to a resonant sequential pulse following a double-diffraction beam splitter.

The efficiency  $\mathcal{E}_{\pm 1}^0$  of the first-order double Raman beam-splitter process sketched in Fig. 1(b) is shown in Fig. 2 as a function of the pulse duration  $\Delta\tau$  and the width of the initial wave function  $\Delta\phi$ . For short pulse durations (i.e. in the Raman-Nath regime) diffraction into higher off-resonant orders becomes important and the efficiency of the beam-splitting process drops. For longer pulses, an efficiency close to unity demonstrates that diffraction in the Bragg-type regime leads to the targeted beam splitter. However, the longer the pulse, the more dominant the Doppler detuning becomes, which leads to velocity selectivity and the diffraction efficiency drops for broad momentum distributions. The red dashed line denotes the optimal pulse duration  $\Delta\tau_{\text{opt}}$  at intermediate times in the quasi-Bragg regime [35] and with highest efficiency for a broad range of different momentum widths  $\Delta\phi$ . For that, we determine for each value  $\Delta\phi$  the pulse duration at which the maximal efficiency occurs and calculate the median over all  $\Delta\phi$ . It will later be used for a comparison between diffraction schemes.

## B. Doppler-detuned Raman diffraction

Atoms in a retroreflective setup with initial momentum  $p_0$  interact predominantly with only one of the two laser pairs because the other pair is Doppler-detuned by  $p_0 K/M$ . Consequently, the double-diffraction process turns into a single-diffraction process, shown by solid arrows in Fig. 3. Note that if the atom is in a superposition of momenta  $\pm p_0$ , two opposite but independent single-diffraction processes occur. However, the off-resonant Doppler-detuned transitions (dashed arrows from  $|e, \pm \hbar K\rangle$  to  $|g, 0\rangle$  in Fig. 3) are still present and cause a shift of the addressed atomic energy levels and by

that detuned Rabi oscillations. A small detuning leads to the *two-photon light shift* [41, 42], while a large detuning reduces the diffraction efficiency. In contrast to Bragg diffraction, for Raman diffraction adiabatic elimination allows to identify the differential energy shift  $\Delta E/\hbar$  for time-independent pulse shapes [43]. For the momenta  $p_0 = n_0\hbar K$  with  $n_0 \in \mathbb{N}$  that are of interest to our study of sequential pulses, one obtains for the widely used box-shaped pulses with Rabi frequency  $\Omega_0$  the following differential energy shift

$$\Delta E/\hbar \equiv \omega_K \delta = \pm \frac{\Omega_0^2}{\omega_K} \frac{2n_0 + 1}{4n_0(n_0 + 1)}. \quad (7)$$

The negative sign corresponds to transitions from  $|g, n_0\hbar K\rangle$  to  $|e, (n_0 + 1)\hbar K\rangle$  while the positive sign corresponds to transitions from  $|e, n_0\hbar K\rangle$  to  $|g, (n_0 + 1)\hbar K\rangle$ . The detuning caused by this shift can be compensated by modifying accordingly the resonance condition from which  $\Delta\omega$  is obtained. Box-shaped pulses are commonly employed for sequential pulses, as they are easy to implement experimentally and have shorter durations compared to Gaussian pulses, while they can maintain a high diffraction efficiency.

To demonstrate this effect, we consider in the following  $p_0 = \pm\hbar K$ , depicted in Fig. 3, and  $p_0 = \pm 2\hbar K$  for box shaped pulses i.e.  $\Omega(t) = \Omega_0$ . The pulse duration  $\tau$  corresponds to the temporal length of the box and differs significantly from the width  $\Delta\tau$  of a Gaussian pulse.

The resonance condition for transition  $|e, \pm\hbar K\rangle \rightarrow |g, \pm 2\hbar K\rangle$ , i.e.  $p_0 = \pm\hbar K$  as depicted in Fig. 3 is given by

$$\Delta\omega = \omega_{eg} - 3\omega_K + \Delta E/\hbar = \omega_{eg} - (3 - \delta)\omega_K \quad (8)$$

with  $\delta = 3\Omega_0^2/(8\omega_K^2)$ . The system of differential equations in an appropriate rotating frame reduces then to an effective two-level system without light shifts:

$$\begin{pmatrix} \dot{e}_{\pm 1} \\ \dot{g}_{\pm 2} \end{pmatrix} = i\Omega_0 \begin{pmatrix} 0 & e^{\mp i\omega_{\text{DT}} t} \\ e^{\pm i\omega_{\text{DT}} t} & 0 \end{pmatrix} \begin{pmatrix} e_{\pm 1} \\ g_{\pm 2} \end{pmatrix}. \quad (9)$$

Keeping in mind the differences between single and double diffraction, we now investigate  $\pi$  pulses by choosing

$$A = \pi = 2\Omega_0\tau. \quad (10)$$

Equation (9) is analytically solvable, but to also calculate loss to off-resonant states that inevitably appears beyond the Bragg-type regime, we resort to a numerical treatment.

Similarly, the resonance condition for the transition  $|g, \pm 2\hbar K\rangle \rightarrow |e, \pm 3\hbar K\rangle$  with  $p_0 = \pm 2\hbar K$  takes the form

$$\Delta\omega = \omega_{eg} + (5 + \delta)\omega_K \quad (11)$$

with  $\delta = -5\Omega_0^2/(24\omega_K^2)$ . It can be reduced to a two-level-system between  $|g, \pm 2\hbar K\rangle$  and  $|e, \pm 3\hbar K\rangle$  similar to Eq. (9).

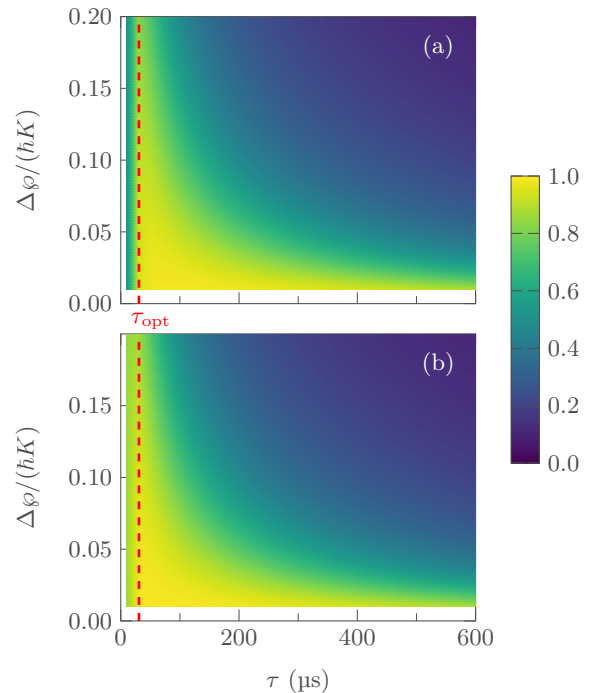


FIG. 4. Efficiency for Doppler-detuned box shaped pulses for varying width of the initial wave function  $\Delta\varphi$  and pulse duration  $\tau$ . In panel (a) the process  $|e, \pm\hbar K\rangle \rightarrow |g, \pm 2\hbar K\rangle$  and in panel (b) the process  $|g, \pm 2\hbar K\rangle \rightarrow |e, \pm 3\hbar K\rangle$  is shown. In the Raman-Nath regime both processes show transitions into other diffraction orders that reduce for increasing  $p_0$ , which makes the pulse in panel (b) more efficient.

Using the resonance condition Eq. (8), we calculate the diffraction efficiency  $\mathcal{E}_{\pm 1}^1$  for the Doppler-detuned transition  $|e, \pm\hbar K\rangle \rightarrow |g, \pm 2\hbar K\rangle$  and using the resonance condition Eq. (11) to calculate the efficiency  $\mathcal{E}_{\pm 1}^2$  for the transition  $|g, \pm 2\hbar K\rangle \rightarrow |e, \pm 3\hbar K\rangle$  with an analogous numerical treatment as discussed in Sec. II A 1. The only differences are the modified resonance conditions and box shaped pulses i.e.  $\Omega(t) = \Omega_0$ . Moreover, the initial wave packet is a superposition of two Gaussians centered at  $\pm p_0$  described by

$$\psi_i(p_i) \propto \exp\left[-\frac{(p_i - p_0)^2}{(4\Delta\varphi^2)}\right] + \exp\left[-\frac{(p_i + p_0)^2}{(4\Delta\varphi^2)}\right]. \quad (12)$$

Figure 4(a) shows the efficiency for  $p_0 = \pm\hbar K$  and Fig. 4(b) the efficiency for  $p_0 = \pm 2\hbar K$  defined through Eq. (6) as a function of the width of the initial wave function  $\Delta\varphi$  and the pulse duration  $\tau$ . Although using different pulse shapes, we observe similar to Fig. 2 diffraction to spurious orders in the Raman-Nath regime and therefore a significant loss of efficiency for short pulses. Since the spurious grating is increasingly off-resonant the larger the initial momentum [36], the Raman-Nath regime is less important for the transition  $|g, \pm 2\hbar K\rangle \rightarrow |e, \pm 3\hbar K\rangle$  compared to the transition  $|e, \pm\hbar K\rangle \rightarrow |g, \pm 2\hbar K\rangle$ .

We compare in Fig. 5 the efficiency obtained with the optimal pulse duration  $\tau_{\text{opt}} \cong 30.7\mu\text{s}$  for the two



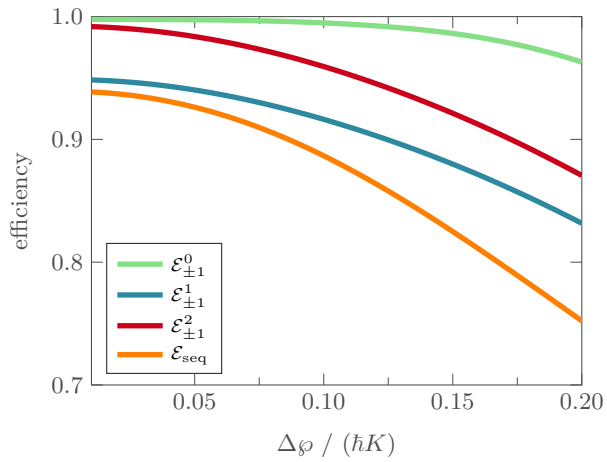


FIG. 5. Diffraction efficiency for the three individual first-order pulses and their sequential application, obtained with the optimal pulse durations. The efficiency  $\mathcal{E}_{\pm 1}^0$  for the double-Raman beam splitter with Gaussian pulse shape corresponds to the cut along the red dashed line in Fig. 2, the efficiencies of the Doppler-detuned and box-shaped single-diffraction mirror pulses  $\mathcal{E}_{\pm 1}^1$  and  $\mathcal{E}_{\pm 1}^2$  to the cuts along the red dashed lines in the two panels of Fig. 4. They differ because of the different diffraction geometries (Doppler-detuned single or double diffraction) as well as the pulse shape employed (Gaussian or box). The efficiency  $\mathcal{E}_{\text{seq}}$  of the sequential application of the three pulses is lower than the efficiency of the individual processes.

effective single-diffraction pulses to that of the double-diffraction beam splitter (i.e., the cuts along the red dashed lines in Figs. 2 and 4). Since the Raman-Nath regime is suppressed for Gaussian pulses, we observe that the double-diffraction beam splitter has the best efficiency for all momentum widths. Off-resonant couplings are suppressed by a Doppler detuning that scales with the initial momentum [36] and therefore affect the transition  $|e, \pm \hbar K\rangle \rightarrow |g, \pm 2\hbar K\rangle$  more than the subsequent process with higher initial momentum. Hence, the first sequential pulse has the lowest efficiency of the individual pulses. However, these two diffraction types differ significantly in their geometry (single versus double diffraction) as well as in the applied pulse shape, which makes a direct comparison difficult.

### C. Three sequential pulses

In this section we use the diffraction processes discussed in Sections II A and II B to perform a pulse sequence transferring population from the state  $|g, 0\rangle$  to an equal-amplitude superposition of  $|e, \pm 3\hbar K\rangle$ . Raman pulses for a double geometry have already been experimentally realized, however only for the transition from  $|0\rangle$  to  $|2\hbar K\rangle$  [12]. A double-diffraction beam splitter with a Gaussian pulse shape transfers the initial wave function from  $|g, 0\rangle$  to  $|e, \pm \hbar K\rangle$ . Two subsequent box-

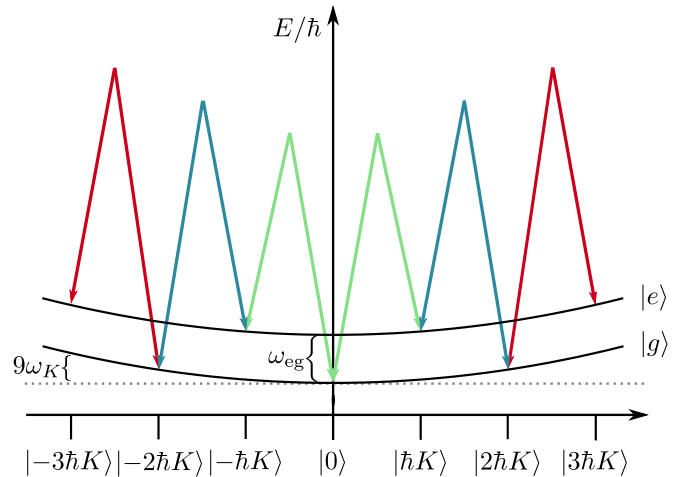


FIG. 6. Energy-momentum diagram that shows the resonant processes of a sequence consisting of a double-diffraction beam splitter (green arrows) and two subsequent Doppler-detuned single-diffraction pulses (blue and red arrows). The initial wave packet is transferred from  $|g, 0\rangle$  to  $|e, \pm \hbar K\rangle$  via the states  $|e, \pm \hbar K\rangle$  and  $|g, \pm 2\hbar K\rangle$ .

shaped and Doppler-detuned effective single-diffraction pulses transfer the population further to  $|g, \pm 2\hbar K\rangle$  and  $|e, \pm 3\hbar K\rangle$  see Fig. 6. The combination of Gaussian and box-shaped pulses in the sequence allows to benefit from their particular advantages regarding experimental duration and transfer efficiency. Each pulse induces first-order diffraction and requires an adjustment of the laser frequencies to fulfill the corresponding resonance conditions from Eqs. (2), (8) and (11). We use the optimal pulse durations  $\Delta\tau_{\text{opt}} \cong 8.8 \mu\text{s}$  and  $\tau_{\text{opt}} \cong 30.7 \mu\text{s}$  obtained in Section II A and Section II B for the individual pulses.

This sequence of optimal pulses leads to a momentum transfer of  $3\hbar K$  and its efficiency  $\mathcal{E}_{\text{seq}}$  is shown in Fig. 5. It is obtained from Eq. (6) by integrating over the population in the states  $|e, \pm 3\hbar K\rangle$  after the sequence and it is slightly larger than the product of the individual efficiencies  $\mathcal{E}_{\pm 1}^0 \mathcal{E}_{\pm 1}^1 \mathcal{E}_{\pm 1}^2$ .

Compared to the three individual pulses shown in the figure, the efficiency of the sequence  $\mathcal{E}_{\text{seq}}$  is lower. In fact, it is mainly limited by the lowest efficiency  $\mathcal{E}_{\pm 1}^1$  of the first sequential pulse. Moreover, the width of the diffracted wave function after each step of the sequence is iteratively reduced due to velocity selectivity.

## III. THIRD-ORDER DIFFRACTION

Instead of three sequential pulses we focus in this section on only one pulse that relies on third-order diffraction to achieve the same momentum transfer of  $\pm 3\hbar K$ . As Fig. 7 shows, the two laser pairs with frequencies  $\omega_b$  and  $\omega_r$  induce a six-photon diffraction process and transfer the population from  $|g, 0\rangle$  to  $|e, \pm 3\hbar K\rangle$ . The interme-

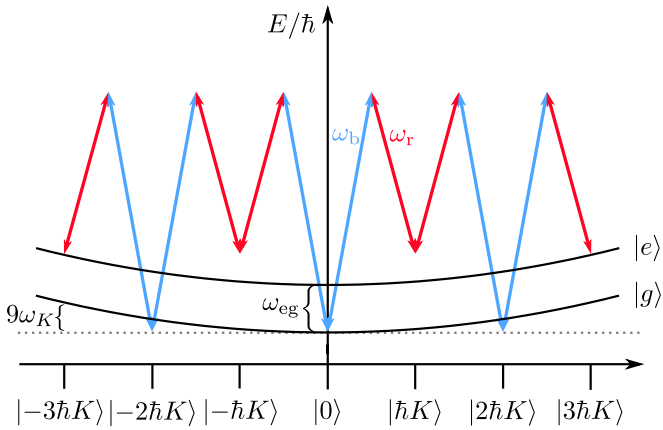


FIG. 7. Energy-momentum diagram for a double Raman six-photon diffraction process. Two laser pairs (red and blue arrows) induce the transition. The first and second scattering process, each a two-photon process, are off-resonant. Thus, the transition from  $|g, 0\rangle$  to  $|e, \pm 3\hbar K\rangle$  occurs by populating the states  $|e, \pm \hbar K\rangle$  and  $|g, \pm 2\hbar K\rangle$  only virtually.

mediate two-photon processes are off-resonant and thus, the states  $|e, \pm \hbar K\rangle$  and  $|g, \pm 2\hbar K\rangle$  are only virtually populated.

### 1. Resonance condition and pulse area

In such a third-order process, the atom gains due to its quadratic dispersion relation a kinetic energy of  $9\hbar\omega_K$ , which leads for  $p_0 = 0$  to the following modified resonance condition:

$$\Delta\omega = \omega_{\text{eg}} + (9 + \delta)\omega_K. \quad (13)$$

Here, we included the factor  $\omega_K\delta$  to compensate for possible energy shifts similar to the Doppler-detuned diffraction processes in Section II B. While these shifts can be derived for higher-order single-Bragg diffraction with *box-shaped* pulses through conventional adiabatic elimination of the intermediate states, the two counterpropagating optical lattices in double Raman diffraction prevent a straightforward application of the procedure [44], even though the technique can be generalized [45] to our case using Floquet theory. Similarly, we apply the method of averaging [46, 47] that has already proven useful for double Bragg diffraction [2] to arrive at

$$\omega_K\delta = -\frac{9\Omega_0^2}{16\omega_K}. \quad (14)$$

Through this procedure, we also find an effective Rabi frequency for the third-order process that scales with  $\Omega_0^3/\omega_K^2$  and connect it to the effective pulse area  $A$

$$A = \frac{\pi}{2} = \frac{\sqrt{2}\Omega_0^3}{32\omega_K^2}\tau. \quad (15)$$

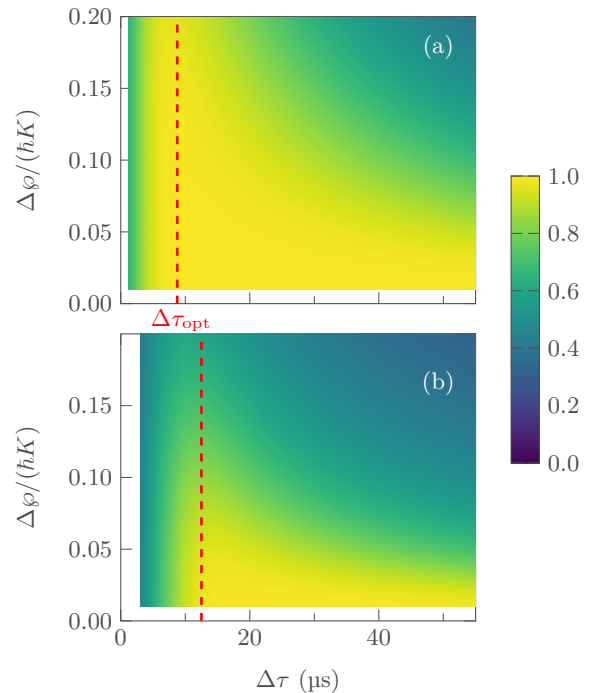


FIG. 8. Comparison of the efficiency for a first-order beam splitter  $\mathcal{E}_{\pm 1}^0$  and a third-order beam splitter  $\mathcal{E}_{\pm 3}^0$  for different widths of the initial wave function  $\Delta\varphi$  and pulse durations  $\Delta\tau$ . Panel (a) recalls the results for the first-order efficiency for times up to  $60\mu\text{s}$  from Fig. 2 and panel (b) shows the simulated efficiency for third-order diffraction on the same time scale. While first-order diffraction is more efficient for a broad range of pulse durations in a Bragg-type regime, third-order diffraction is limited by two main effects: In the Bragg-type regime, higher-order diffraction is intrinsically limited by velocity selectivity, while for small pulse durations losses into intermediate state appear.

However, adiabatic-elimination like the method of averaging cannot be trivially extended to other pulse shapes. Since we focus in this article on *Gaussian* pulse shapes for double diffraction, we determine the energy shifts

$$\omega_K\delta = \beta \frac{\Omega_0^2}{\omega_K} \quad (16)$$

as well as the connection to the modified Rabi frequency and pulse area

$$A = \int dt \alpha \frac{\Omega^3(t)}{\omega_K^2}. \quad (17)$$

through a numerical optimization of the diffraction efficiency with the MATLAB function *fminsearch* by determining the optimization parameters  $\beta$  and  $\alpha$ . For our range of initial momentum widths and pulse durations, we find that  $\beta \in [-0.75, -0.42]$  and  $\alpha \in [0.025, 0.072]$  do not deviate much from the corresponding analytical value for box-shaped pulses given by Eqs. (14) and (15).

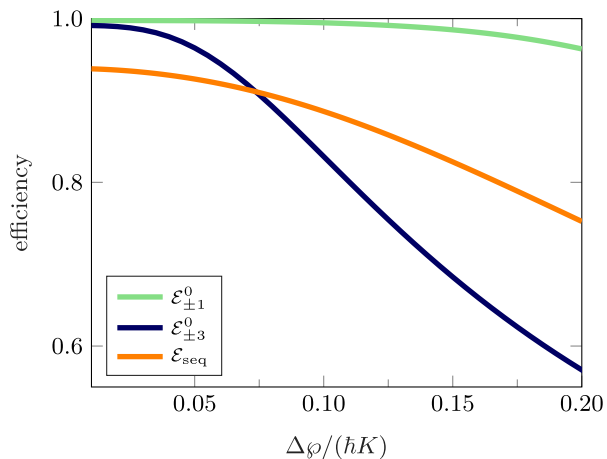


FIG. 9. Efficiency at optimal pulse duration for different widths of the initial wave function  $\Delta\varphi$  for the first- and third-order beam splitter as well as the sequence. Due to different regimes of pulse durations the first-order beam splitter is less velocity selective than its third-order counterpart. For small  $\Delta\varphi$  the third-order pulse is more efficient than the sequence, which makes it an interesting alternative for the diffraction of narrow wave packets like BECs.

## 2. Comparison to first-order and sequential pulses

We recall in Fig. 8(a) the efficiency of the first-order beam-splitter pulse  $\mathcal{E}_{\pm 1}^0$  from Fig. 2 and compare it to the corresponding third-order beam splitter efficiency  $\mathcal{E}_{\pm 3}^0$  in Fig. 8(b) for different widths of the initial wave function  $\Delta\varphi$  and pulse durations  $\Delta\tau$ . As expected, third-order diffraction requires longer pulse durations, or, higher intensities for an efficient transfer since the population has to overcome two intermediate and off-resonant states. Moreover, velocity selectivity increases with the order of the diffraction process. Indeed, for  $n$ th-order diffraction the velocity spread associated with velocity-selectivity effects is proportional to  $1/n$  because the effective Doppler detuning is given in that case by  $n\omega_D = npK/m$ . For small pulse durations losses into the intermediate states appear, especially into  $|g, \pm 2\hbar K\rangle$  since it is the least off-resonant intermediate state as shown by Fig. 7, while for larger pulse durations the loss of the efficiency of the diffracted population is mainly caused by velocity selectivity. Again, there exists a pulse duration  $\Delta\tau_{\text{opt}}$  at which the atoms are diffracted most efficiently (red dashed line). When comparing these graphs, it seems that third-order diffraction seems to be less efficient than the first-order pulse.

In Fig. 9 we compare the efficiencies with optimal pulse duration for the first-order ( $\Delta\tau_{\text{opt}} \cong 8.8 \mu\text{s}$ ) and third-order beam splitter ( $\Delta\tau_{\text{opt}} \cong 13.3 \mu\text{s}$ ), as well as the sequence introduced in Section II C as a function of the widths of the initial wave function  $\Delta\varphi$ . As already observed above, the first-order beam splitter has a much higher efficiency than its third-order counterpart, which

can be understood in terms of velocity selectivity and loss to intermediate states. However, if the targeted states are  $|e, \pm 3\hbar K\rangle$ , the third-order pulse has to be compared to the sequence of three first-order pulses rather than just the initial beam splitter. Indeed, the third-order pulse shows high efficiency for small momentum distributions, that exceeds the efficiency of the sequential application of three individual pulses. Even though the efficiency of the sequence could be improved by using Gaussian pulses throughout the sequence instead of only for the initial beam splitter, this would come at the cost of an even longer duration of the whole sequence. Consequently, third-order diffraction might be an interesting tool for the diffraction of wave packets with a narrow momentum distribution like BECs, since it allows to reduce the complexity of the experiment. In general, each transition of a sequence might introduce spurious phase contributions [48] and using less pulses may facilitate the suppression of some uncertainties connected to frequency chirps [49–51]. Furthermore, the overall duration of a single pulse can become shorter than that of a corresponding sequence of pulses, which might be particularly appealing for very compact set-ups [52] intended for real-world applications [53].

## IV. CONCLUSIONS

Double Raman diffraction allows in principle for resonant diffraction of odd orders, i.e. of order  $2n + 1$  with  $n = 0, 1, 2, \dots$ . Higher diffraction orders come along with a higher velocity selectivity than first-order pulses. Moreover, higher intensities are necessary to overcome the intermediate states to achieve the optimal diffraction efficiency. However, when comparing third-order diffraction with a sequence consisting of three first-order pulses we find that third-order pulses diffract narrow momentum distributions like the ones associated with BECs more efficiently. The efficiency of our sequence, consisting of one Gaussian and two box-shaped pulses, could be improved by using Gaussian pulses only but at the cost of a significantly higher duration of the sequence.

Third-order Raman mirrors can also be realized but suffer further limitations like losses into the central state  $|g, 0\rangle$ , a feature intrinsic to double-diffraction mirrors [36]. However, the difficulties can be overcome by replacing the mirror pulse through Bragg diffraction of sixth order from a standing wave, a scheme not investigated in this study.

In addition to the possibility of higher-order diffraction, the symmetry of double-Raman pulses suppresses laser phase noise. Thus, it can be applied within LMT sequences together with Bragg diffraction or combined with Bloch oscillations.

Hence, double Raman diffraction is a versatile tool for LMT techniques with the same flexibility and limitations as double Bragg diffraction. Not only does it occur naturally in microgravity or horizontal setups, it can also be

combined perfectly with other LMT applications [22] to enhance the sensitivity of atom interferometers.

### ACKNOWLEDGMENTS

We thank M. Gebbe, M. Gersemann, C. M. Carmesin, A. Friedrich and the whole QUANTUS group in Ulm as well as our partners of the QUANTUS collaboration for helpful discussions. This work is supported by the German Aerospace Center (Deutsches Zentrum für Luft- und Raumfahrt, DLR) with funds provided by the Federal Ministry for Economic Affairs and Energy (Bundesministerium für Wirtschaft und Energie, BMWi) due to an enactment of the German Bundestag under Grant Nos. DLR 50WM1556 (QUANTUS IV), DLR 50WM1956 (QUANTUS V), DLR 50WP1700 and 50WP1705 (BEC-CAL), 50RK1957 (QGYRO) as well as the Association of German Engineers (Verein Deutscher Ingenieure, VDI) with funds provided by the Federal Ministry of Education and Research (Bundesministerium für Bildung und Forschung, BMBF) under Grant No. VDI 13N14838 (TAIOL). E. G. thanks the German Research Foundation (Deutsche Forschungsgemeinschaft, DFG) for a Mercator Fellowship within CRC 1227 (DQ-mat). We thank the Ministry of Science, Research and Art Baden-Württemberg (Ministerium für Wissenschaft, Forschung und Kunst Baden-Württemberg) for financially supporting the work of IQ<sup>ST</sup>.

### APPENDIX: GENERAL EQUATIONS

In the following we discuss the differential equations for double Raman diffraction in their most general form,

i.e. we do not focus on a specific resonance condition. A truncated version can also be found in Ref [54].

The differential equations are derived within a rotating wave approximation [55] and the optically excited state is eliminated by adiabatic elimination [56–58]. Moreover, the equations are in an interaction picture with respect to the free evolution of the atoms and we assume that the laser phases vanish. They read

$$\begin{aligned} \dot{g}_n &= i\Omega e^{-i[\omega_D + \omega_{eg} - \Delta\omega + \omega_{AC} + (1+2n)\omega_K]t} e_{n+1} \\ &+ i\Omega e^{-i[-\omega_D + \omega_{eg} - \Delta\omega + \omega_{AC} + (1-2n)\omega_K]t} e_{n-1} \end{aligned} \quad (18a)$$

$$\begin{aligned} \dot{e}_{n+1} &= i\Omega e^{-i[\omega_D - \omega_{eg} + \Delta\omega - \omega_{AC} + (3+2n)\omega_K]t} g_{n+2} \\ &+ i\Omega e^{-i[-\omega_D - \omega_{eg} + \Delta\omega - \omega_{AC} - (1+2n)\omega_K]t} g_n \end{aligned} \quad (18b)$$

Hence, the probability amplitudes of the ground  $g_n \equiv g(p + n\hbar K)$  and excited state  $e_n \equiv e(p + n\hbar K)$  form a system of coupled differential equations. The coupling strength  $\Omega(t)$  is determined by the laser intensity and the pulse shape. The frequency difference between ground state and excited state is given by  $\omega_{eg}$  while the Doppler frequency  $\omega_D$  denotes the deviation from a resonant momentum within a wave packet and thus, acts as a detuning. The recoil frequency is given by  $\omega_K$  and the AC Stark effect by  $\omega_{AC}$ . The adjustment of the laser frequency difference  $\Delta\omega$  allows to perform resonant transitions between certain momentum states. Inserting the resonance condition Eq. (2) into Eq. (18) leads for example to first-order diffraction as discussed in Sec. II. A feature of double compared to single diffraction is the possibility to diffract into two directions simultaneously.

- 
- [1] H. Müller, S.-w. Chiow, Q. Long, S. Herrmann, and S. Chu, “Atom Interferometry with up to 24-Photon-Momentum-Transfer Beam Splitters,” *Phys. Rev. Lett.* **100**, 180405 (2008).
- [2] E. Giese, A. Roura, G. Tackmann, E. M. Rasel, and W. P. Schleich, “Double Bragg diffraction: A tool for atom optics,” *Phys. Rev. A* **88**, 053608 (2013).
- [3] J. Küber, F. Schmaltz, and G. Birkel, “Experimental realization of double Bragg diffraction: robust beamsplitters, mirrors, and interferometers for Bose-Einstein condensates,” (2016), [arXiv:1603.08826](https://arxiv.org/abs/1603.08826).
- [4] J.-N. Siemß, F. Fitzek, S. Abend, E. M. Rasel, N. Gaaloul, and K. Hammerer, “Analytic theory for Bragg atom interferometry based on the adiabatic theorem,” (2020), [arXiv:2002.04588](https://arxiv.org/abs/2002.04588).
- [5] Q. Hu, J. Yang, Y. Luo, A. Jia, C. Wei, and Z. Li, “A theoretical analysis and determination of the technical requirements for a Bragg diffraction-based cold atom interferometry gravimeter,” *Optik* **131**, 632 – 639 (2017).
- [6] H. Ahlers, H. Müntinga, A. Wenzlawski, M. Krutzik, G. Tackmann, S. Abend, N. Gaaloul, E. Giese, A. Roura, R. Kuhl, C. Lämmerzahl, A. Peters, P. Windpassinger, K. Sengstock, W. P. Schleich, W. Ertmer, and E. M. Rasel, “Double Bragg Interferometry,” *Phys. Rev. Lett.* **116**, 173601 (2016).
- [7] S.-w. Chiow, T. Kovachy, H. Chien, and M. A. Kasevich, “102 $\hbar k$  Large Area Atom Interferometers,” *Phys. Rev. Lett.* **107**, 130403 (2011).
- [8] M. A. Kasevich and S. Chu, “Atomic interferometry using stimulated Raman transitions,” *Phys. Rev. Lett.* **67**, 181–184 (1991).
- [9] S. Kleinert, E. Kajari, A. Roura, and W. P. Schleich, “Representation-free description of light-pulse atom interferometry including non-inertial effects,” *Phys. Rep.* **605**, 1–50 (2015).
- [10] M. A. Kasevich, D. S. Weiss, E. Riis, K. Moler, S. Kasapi, and S. Chu, “Atomic velocity selection using stimulated Raman transitions,” *Phys. Rev. Lett.* **66**, 2297–2300 (1991).
- [11] K. Moler, D. S. Weiss, M. A. Kasevich, and S. Chu, “Theoretical analysis of velocity-selective Raman transitions,” *Phys. Rev. A* **45**, 342–348 (1992).



- [12] T. Lévèque, A. Gauguet, F. Michaud, F. Pereira Dos Santos, and A. Landragin, “Enhancing the Area of a Raman Atom Interferometer Using a Versatile Double-Diffraction Technique,” *Phys. Rev. Lett.* **103**, 080405 (2009).
- [13] J. M. McGuirk, M. J. Snadden, and M. A. Kasevich, “Large area light-pulse atom interferometry,” *Phys. Rev. Lett.* **85**, 4498–4501 (2000).
- [14] P. Berg, S. Abend, G. Tackmann, C. Schubert, E. Giese, W. P. Schleich, F. A. Narducci, W. Ertmer, and E. M. Rasel, “Composite-light-pulse technique for high-precision atom interferometry,” *Phys. Rev. Lett.* **114**, 063002 (2015).
- [15] N. Malossi, Q. Bodart, S. Merlet, T. Lévèque, A. Landragin, and F. Pereira Dos Santos, “Double diffraction in an atomic gravimeter,” *Phys. Rev. A* **81**, 013617 (2010).
- [16] I. Perrin, J. Bernard, Y. Bidet, A. Bonnin, N. Zahzam, C. Blanchard, A. Bresson, and M. Cadoret, “Zero-velocity atom interferometry using a retroreflected frequency-chirped laser,” *Phys. Rev. A* **100**, 053618 (2019).
- [17] L. Zhou, S. Long, B. Tang, X. Chen, F. Gao, W. Peng, W. Duan, J. Zhong, Z. Xiong, J. Wang, Y. Zhang, and M. Zhan, “Test of Equivalence Principle at  $10^{-8}$  Level by a Dual-Species Double-Diffraction Raman Atom Interferometer,” *Phys. Rev. Lett.* **115**, 013004 (2015).
- [18] P. Cladé, S. Guellati-Khélifa, F. Nez, and F. Biraben, “Large Momentum Beam Splitter Using Bloch Oscillations,” *Phys. Rev. Lett.* **102**, 240402 (2009).
- [19] G. D. McDonald, C. C. N. Kuhn, S. Bennetts, J. E. Debs, K. S. Hardman, M. Johnsson, J. D. Close, and N. P. Robins, “ $80\hbar k$  momentum separation with Bloch oscillations in an optically guided atom interferometer,” *Phys. Rev. A* **88**, 053620 (2013).
- [20] S. Abend, M. Gebbe, M. Gersemann, H. Ahlers, H. Müntinga, E. Giese, N. Gaaloul, C. Schubert, C. Lämmerzahl, W. Ertmer, W. P. Schleich, and E. M. Rasel, “Atom-Chip Fountain Gravimeter,” *Phys. Rev. Lett.* **117**, 203003 (2016).
- [21] Z. Pagel, W. Zhong, R. H. Parker, C. T. Olund, N. Y. Yao, and H. Müller, “Symmetric Bloch oscillations of matter waves,” (2019), [arXiv:1907.05994](https://arxiv.org/abs/1907.05994).
- [22] M. Gebbe, S. Abend, J.-N. Siemß, M. Gersemann, H. Ahlers, H. Müntinga, S. Herrmann, N. Gaaloul, C. Schubert, K. Hammerer, C. Lämmerzahl, W. Ertmer, and E. M. Rasel, “Twin-lattice atom interferometry,” (2019), [arXiv:1907.08416](https://arxiv.org/abs/1907.08416).
- [23] T. Kovachy, P. Asenbaum, C. Overstreet, C. A. Donnelly, S. M. Dickerson, A. Sugarbaker, J. M. Hogan, and M. A. Kasevich, “Quantum superposition at the half-metre scale,” *Nature* **528**, 530 (2015).
- [24] R. Geiger, V. Ménot, G. Stern, N. Zahzam, P. Cheinet, B. Battelier, A. Villing, F. Moron, M. Lours, Y. Bidet, A. Bresson, A. Landragin, and P. Bouyer, “Detecting inertial effects with airborne matter-wave interferometry,” *Nat. Commun.* **2**, 474 (2011).
- [25] H. Müntinga, H. Ahlers, M. Krutzik, A. Wenzlawski, S. Arnold, D. Becker, K. Bongs, H. Dittus, H. Duncker, N. Gaaloul, C. Gherasim, E. Giese, C. Grzeschik, T. W. Hänsch, O. Hellmig, W. Herr, S. Herrmann, E. Kajari, S. Kleinert, C. Lämmerzahl, W. Lewoczko-Adamczyk, J. Malcolm, N. Meyer, R. Nolte, A. Peters, M. Popp, J. Reichel, A. Roura, J. Rudolph, M. Schiemanck, M. Schneider, S. T. Seidel, K. Sengstock, V. Tamma, T. Valenzuela, A. Vogel, R. Walser, T. Wendrich, P. Windpassinger, W. Zeller, T. van Zoest, W. Ertmer, W. P. Schleich, and E. M. Rasel, “Interferometry with Bose-Einstein Condensates in Microgravity,” *Phys. Rev. Lett.* **110**, 093602 (2013).
- [26] D. Becker, M. D. Lachmann, S. T. Seidel, H. Ahlers, A. N. Dinkelaker, J. Grosse, O. Hellmig, H. Müntinga, V. Schkolnik, T. Wendrich, A. Wenzlawski, B. Weps, R. Corgier, T. Franz, N. Gaaloul, W. Herr, D. Lüdtke, M. Popp, S. Amri, H. Duncker, M. Erbe, A. Kohfeldt, A. Kubelka-Lange, C. Braxmaier, E. Charron, W. Ertmer, M. Krutzik, C. Lämmerzahl, A. Peters, W. P. Schleich, K. Sengstock, R. Walser, A. Wicht, P. Windpassinger, and E. M. Rasel, “Space-borne Bose-Einstein condensation for precision interferometry,” *Nature* **562**, 391 (2018).
- [27] D. C. Aveline, J. R. Williams, E. R. Elliott, C. Dutenhofer, J. R. Kellogg, J. M. Kohel, N. E. Lay, K. Oudrhiri, R. F. Shotwell, N. Yu, and R. J. Thompson, “Observation of Bose-Einstein condensates in an Earth-orbiting research lab,” *Nature* **582**, 193–197 (2020).
- [28] K. Frye, S. Abend, W. Bartosch, A. Bawamia, D. Becker, H. Blume, C. Braxmaier, S.-w. Chiow, M. A. Efremov, W. Ertmer, P. Fierlinger, N. Gaaloul, J. Grosse, C. Grzeschik, O. Hellmig, V. A. Henderson, W. Herr, U. Israelsson, J. Kohel, M. Krutzik, C. Kürbis, C. Lämmerzahl, M. List, D. Lüdtke, N. Lundblad, J. P. Marburger, M. Meister, M. Mihm, H. Müller, H. Müntinga, T. Oberschulte, A. Papakonstantinou, J. Perovšek, A. Peters, A. Prat, E. M. Rasel, A. Roura, W. P. Schleich, C. Schubert, S. T. Seidel, J. Sommer, C. Spindeldreier, D. Stamper-Kurn, B. K. Stuhl, M. Warner, T. Wendrich, A. Wenzlawski, A. Wicht, P. Windpassinger, N. Yu, and L. Wörner, “The Bose-Einstein Condensate and Cold Atom Laboratory,” (2019), [arXiv:1912.04849](https://arxiv.org/abs/1912.04849).
- [29] D. N. Aguilera, H. Ahlers, B. Battelier, A. Bawamia, A. Bertoldi, R. Bondarescu, K. Bongs, P. Bouyer, C. Braxmaier, L. Cacciapuoti, C. Chaloner, M. Chwalla, W. Ertmer, M. Franz, N. Gaaloul, M. Gehler, D. Gerardi, L. Gesa, N. Gürebeck, J. Hartwig, M. Hauth, O. Hellmig, W. Herr, S. Herrmann, A. Heske, A. Hinton, P. Ireland, P. Jetzer, U. Johann, M. Krutzik, A. Kubelka, C. Lämmerzahl, A. Landragin, I. Lloro, D. Massonnet, I. Mateos, A. Milke, M. Nofrarias, M. Oswald, A. Peters, K. Posso-Trujillo, E. M. Rasel, E. Rocco, A. Roura, J. Rudolph, W. P. Schleich, C. Schubert, T. Schuldt, S. Seidel, K. Sengstock, C. F. Sopuerta, F. Sorrentino, D. Summers, G. M. Tino, C. Trenkel, N. Uzunoglu, W. von Klitzing, R. Walser, T. Wendrich, A. Wenzlawski, P. Weßels, A. Wicht, E. Wille, M. Williams, P. Windpassinger, and N. Zahzam, “STE-QUEST—test of the universality of free fall using cold atom interferometry,” *Classical Quantum Gravity* **31**, 115010 (2014).
- [30] J. M. Hogan, D. M. S. Johnson, S. Dickerson, T. Kovachy, A. Sugarbaker, S.-w. Chiow, P. W. Graham, M. A. Kasevich, B. Saif, S. Rajendran, P. Bouyer, B. D. Seery, L. Feinberg, and R. Keski-Kuha, “An atomic gravitational wave interferometric sensor in low earth orbit (AGIS-LEO),” *Gen. Relativ. Gravitation* **43**, 1953–2009 (2011).
- [31] B. Canuel, S. Abend, P. Amaro-Seoane, F. Badaracco, Q. Beaufiles, A. Bertoldi, K. Bongs, P. Bouyer, C. Braxmaier, W. Chaibi, N. Christensen, F. Fitzek, G. Flouris,

- N. Gaaloul, S. Gaffet, C. L. Garrido Alzar, R. Geiger, S. Guellati-Khelifa, K. Hammerer, J. Harms, J. Hinderer, J. Junca, S. Katsanevas, C. Klempt, C. Kozanitis, M. Krutzik, A. Landragin, I. L. àzaro Roche, B. Leykauf, Y.-H. Lien, S. Loriani, S. Merlet, M. Merzougui, M. Nofrarias, P. Papadakos, F. Pereira, A. Peters, D. Plexousakis, M. Prevedelli, E. M. Rasel, Y. Rogister, S. Rosat, A. Roura, D. O. Sabulsky, V. Schkolnik, D. Schlippert, C. Schubert, L. Sidorenkov, J.-N. Siemß, C. F. Sopaerta, F. Sorrentino, C. Struckmann, G. M. Tino, G. Tsagkatakis, A. Viceré, W. von Klitzing, L. Wörner, and X. Zou, “ELGAR – a European Laboratory for Gravitation and Atom-interferometric Research,” (2019), [arXiv:1911.03701](https://arxiv.org/abs/1911.03701).
- [32] C. Schubert, D. Schlippert, S. Abend, E. Giese, A. Roura, W. P. Schleich, W. Ertmer, and E. M. Rasel, “Scalable, symmetric atom interferometer for infrasound gravitational wave detection,” (2019), [arXiv:1909.01951](https://arxiv.org/abs/1909.01951).
- [33] Y. Torii, Y. Suzuki, M. Kozuma, T. Sugiura, T. Kuga, L. Deng, and E. W. Hagley, “Mach-Zehnder Bragg interferometer for a Bose-Einstein condensate,” *Phys. Rev. A* **61**, 041602 (2000).
- [34] E. Giese, “Mechanisms of matter-wave diffraction and their application to interferometers,” *Fortschr. Phys.* **63**, 337–410 (2015).
- [35] H. Müller, S.-w. Chiow, and S. Chu, “Atom-wave diffraction between the Raman-Nath and the Bragg regime: Effective Rabi frequency, losses, and phase shifts,” *Phys. Rev. A* **77**, 023609 (2008).
- [36] S. Hartmann, J. Jenewein, E. Giese, S. Abend, A. Roura, E. M. Rasel, and W. P. Schleich, “Regimes of atomic diffraction: Raman versus Bragg diffraction in retro-reflective geometries,” *Phys. Rev. A* **101**, 053610 (2020).
- [37] P. L. Gould, G. A. Ruff, and D. E. Pritchard, “Diffraction of atoms by light: The near-resonant Kapitza-Dirac effect,” *Phys. Rev. Lett.* **56**, 827–830 (1986).
- [38] M. Kozuma, L. Deng, E. W. Hagley, J. Wen, R. Lutwak, K. Helmerson, S. L. Rolston, and W. D. Phillips, “Coherent Splitting of Bose-Einstein Condensed Atoms with Optically Induced Bragg Diffraction,” *Phys. Rev. Lett.* **82**, 871–875 (1999).
- [39] S. S. Szigeti, J. E. Debs, J. J. Hope, N. P. Robins, and J. D. Close, “Why momentum width matters for atom interferometry with Bragg pulses,” *New J. Phys.* **14**, 023009 (2012).
- [40] A. Neumann, R. Walser, and W. Nörtershäuser, “Raman velocity filter as a tool for collinear laser spectroscopy,” *Phys. Rev. A* **101**, 052512 (2020).
- [41] O. Carraz, R. Charrire, M. Cadoret, N. Zahzam, Y. Bidel, and A. Bresson, “Phase shift in an atom interferometer induced by the additional laser lines of a Raman laser generated by modulation,” *Phys. Rev. A* **86**, 033605 (2012).
- [42] E. Giese, A. Friedrich, S. Abend, E. M. Rasel, and W. P. Schleich, “Light shifts in atomic Bragg diffraction,” *Phys. Rev. A* **94**, 063619 (2016).
- [43] A. Gauguier, T. E. Mehlstäubler, T. Lévêque, J. Le Gouët, W. Chaibi, B. Canuel, A. Clairon, F. Pereira Dos Santos, and A. Landragin, “Off-resonant Raman transition impact in an atom interferometer,” *Phys. Rev. A* **78**, 043615 (2008).
- [44] V. Paulisch, H. Rui, H. K. Ng, and B.-G. Englert, “Beyond adiabatic elimination: A hierarchy of approximations for multi-photon processes,” *The European Physical Journal Plus* **129**, 12 (2014).
- [45] M. Sanz, E. Solano, and Í. Egusquiza, “Beyond adiabatic elimination: Effective Hamiltonians and singular perturbation,” in *Applications+ Practical Conceptualization+ Mathematics= fruitful Innovation* (Springer, 2016) pp. 127–142.
- [46] N. N. Bogoliubov and Y. A. Mitropolsky, *Asymptotic methods in the theory of non-linear oscillations*, Vol. 10 (CRC Press, 1961).
- [47] P. Kling, *Theory of the Free-Electron Laser: from classical to quantum*, Ph.D. thesis, Universität Ulm (2018).
- [48] B. Décamps, M. Bordoux, J. Alibert, B. Allard, and A. Gauguier, “Phase response of atom interferometers based on sequential Bragg diffractions,” *J. Phys. B: At., Mol. Opt. Phys.* **52**, 015003 (2018).
- [49] P. Gillot, B. Cheng, S. Merlet, and F. Pereira Dos Santos, “Limits to the symmetry of a Mach-Zehnder-type atom interferometer,” *Phys. Rev. A* **93**, 013609 (2016).
- [50] R. Karcher, F. Pereira Dos Santos, and S. Merlet, “Impact of direct-digital-synthesizer finite resolution on atom gravimeters,” *Phys. Rev. A* **101**, 043622 (2020).
- [51] B. Cheng, P. Gillot, S. Merlet, and F. Pereira Dos Santos, “Influence of chirping the Raman lasers in an atom gravimeter: Phase shifts due to the Raman light shift and to the finite speed of light,” *Phys. Rev. A* **92**, 063617 (2015).
- [52] K. D. Nelson, C. D. Fertig, P. Hamilton, J. M. Brown, B. Estey, H. Müller, and R. L. Compton, “Guided matter wave inertial sensing in a miniature physics package,” *Applied Physics Letters* **116**, 234002 (2020).
- [53] K. Bongs, M. Holynski, J. Vovrosh, P. Bouyer, G. Condon, E. M. Rasel, C. Schubert, W. P. Schleich, and A. Roura, “Taking atom interferometric quantum sensors from the laboratory to real-world applications,” *Nature Reviews Physics*, 1–9 (2019).
- [54] T. Lévêque, *Development of a high sensitivity cold atom gyroscope based on a folded geometry*, Ph. D. thesis, Université Pierre et Marie Curie - Paris VI (2010).
- [55] W. P. Schleich, *Quantum Optics in Phase Space* (Wiley-VCH, Weinheim, 2001).
- [56] A. F. Bernhard and B. W. Shore, “Coherent atomic deflection by resonant standing waves,” *Phys. Rev. A* **23**, 1290–1301 (1981).
- [57] M. Marte and S. Stenholm, “Multiphoton resonances in atomic Bragg scattering,” *Appl. Phys. B: Lasers Opt.* **54**, 443–450 (1992).
- [58] E. Brion, L. H. Pedersen, and K. Mølmer, “Adiabatic elimination in a lambda system,” *J. Phys. A: Math. Theor.* **40**, 1033–1043 (2007).